Research Article | Vol. 27, No. 25 / 9 December 2019 / Optics Express 36601
Optics EXPRESS

Magnetically enhanced luminescence of CdSe/ZnS quantum dot light-emitting diodes using circular ferromagnetic Co/Pt multilayer disks

JANG-HWAN HAN,[1] NA-YEONG KIM,[2] SANG-JO KIM,[1] WONYOUNG KWAK,[1] BEONGKI CHO,[1,2] SEONG-JU PARK,[1,2] AND DONG-SEON LEE[3,*]

[1]School of Materials Science and Engineering, Gwangju Institute of Science and Technology, Gwangju 61005, South Korea
[2]Department of Nanobio Materials and Electronics, Gwangju Institute of Science and Technology, Gwangju 61005, South Korea
[3]School of Electrical Engineering and Computer Science, Gwangju Institute of Science and Technology, Gwangju 61005, South Korea
*dslee66@gist.ac.kr

Abstract: We investigate the effect of a magnetic field on red, green, and blue CdSe/ZnS quantum dot light-emitting diodes (QDLEDs). Circular multilayer ferromagnetic cobalt/platinum (Co/Pt) disks are deposited on a MgF_2 layer covering an Al electrode, and a perpendicular magnetic field is applied to the QDs in the active layer. Carriers injected into the active layer are then trapped and efficiently recombined inside the QDs because of strong carrier localization caused by the perpendicular magnetic field. The luminescence of the QDLEDs in the multilayer increases by 33.31% at 7.5 V, 22.34% at 7.5 V, and 16.73% at 7.0 V compared with that of QDLEDs without the multilayer. The time-resolved photoluminescence of all the QDLEDs also indicates that their increased luminescence results from improved radiative recombination through the stronger carrier localization in the QDs.

1. Introduction

Quantum dot light-emitting diodes (QDLEDs) have drawn a lot of attention owing to their narrow bandwidth, wide emission spectrum, high color purity, good photo stability, and low cost [1,2]. These advantages make QDLEDs superior for replacing organic light-emitting diodes (OLEDs) or polymer light-emitting diodes (PLEDs). Because of these advantages, QDLEDs have been applied to flexible light sources, optoelectronics, and other biomedical fields [3,4]. However, QDLEDs still have low electroluminescence (EL) efficiency because of low carrier injection [5], high nonradiative energy transfer [6], and poor out-coupling efficiency [7]. Surface or interface defect-related trapping and carrier release through thermal escape also cause low QDLED efficiency [8–10]. Overcoming carrier release requires localizing the carriers inside the QDs to attain a high efficiency. However, there have not been many studies on preventing carrier release from a QD before radiative recombination. Although methods such as shell thickness optimization [11] and multi-shell structure [10] have been introduced to enhance carrier confinement in the QD core region, they require a precise and optimized process for each QD core and shell material.

The effect of a magnetic field on QDs has been reported in a few studies [12,13]. These studies suggest the possibility of increasing optical properties by applying an external magnetic field to a QD. They found that an external magnetic field changes photoluminescence (PL) properties such as peak position, full width at half maximum (FWHM), and luminescence intensity. The changes

#378596 https://doi.org/10.1364/OE.27.036601
Journal © 2019 Received 23 Sep 2019; revised 2 Nov 2019; accepted 5 Nov 2019; published 2 Dec 2019

Optics EXPRESS

in optical and electrical properties are due to carrier trajectory changes and increased carrier localization by the external magnetic field. Larsson et al. reported that a strong carrier localization prevented carrier release when a magnetic field was applied to a QD [12]. Furthermore, the change in carrier trajectory due to the magnetic field pushes the carriers in a lateral direction and consequently increases the carrier population around the QDs. As a result, the external magnetic field enhances the PL intensity. The changes in optical and electrical characteristics caused by magnetic fields have been analyzed through semiconductor devices such as Hall-effect sensors [14,15], a GaAs/AlGaAs heterostructure [16], InGaAs/GaAs, [17] and InGaN/GaN multiple quantum wells (MQWs) [18,19]. These results indicate that the magnetic field easily traps the carriers in local potential minima such as the In-rich region, and PL is increased by the increase in radiative recombination rate at the potential minima. External magnetic fields have also been used to improve performance of OLEDs [20–22]. The increase of PL intensity in inorganic and organic LEDs is also attributed to the carrier trajectory change from straight to helical due to the magnetic field. In particular, the magnetic field gradient generated by magnetic structures directly deposited on devices effectively alters the carrier trajectory via scattering and trapping [14,15,19]. However, all previous studies on QDs have been under the conditions of a uniform external magnetic field and low-temperature environment. There is no published report on the effect of the magnetic field gradient from directly deposited magnetic structures on QDLEDs.

In this study, we demonstrated that QDLED luminescence can be increased using the perpendicular magnetic field and magnetic field gradient from directly deposited circular ferromagnetic Co/Pt multilayer (FCPM) disks on a MgF_2 capping layer. Using the perpendicular magnetic field and its gradient, carriers can be spread further in the lateral direction of the active layer and strongly localized in the QD, resulting in enhanced radiative recombination. During the measurement, we observed that with circular FCPM disks the luminescence of a red QDLED increases more than the luminescences of green and blue QDLEDs. To further understand the magnetic field gradient effect in QDLEDs, we performed time-resolved PL (TR-PL) measurements on the QDLEDs with and without the circular FCPM disks.

2. Method

Figures 1(a) to 1(g) illustrate the fabrication sequence for the QDLEDs with circular FCPM disks. First, a patterned indium tin oxide (ITO) glass substrate was sonicated for 10 min in each of the following sequentially: acetone, deionized water, and isopropyl alcohol (IPA). After cleaning, the ITO glass substrate was exposed to an ultraviolet ozone treatment for 20 min (Fig. 1(a)). Then, PEDOT:PSS (Clevios P VP AI 4083, H. C. Stark) was spin-coated on the substrate at 5,000 rpm for 40 sec and baked at 140 °C for 10 min under ambient conditions. Subsequently, poly[N,N'-bis(4-butylphenyl)-N,N'-bis(phenyl)benzidine] (poly-TPD) (American Dye Source) was dissolved in chlorobenzene with a concentration of 10 $mg \cdot mL^{-1}$, spin-coated onto the PEDOT:PSS-coated ITO glass at a rate of 4,000 rpm for 40 sec in a nitrogen-(N_2-)filled glove box, and sequentially baked at 110 °C for 20 min (Fig. 1(b)). Red, green, and blue-emitting CdSe/ZnS core-shell QDs were purchased from Nanosquare. The QDs were dispersed in toluene with a concentration of 10 $mg \cdot mL^{-1}$ and used in QDLED fabrication without any purification. The core and shell materials of the red, green, and blue dots were the same in this study. The differences were the core sizes and shell thicknesses. (In general, when the QD composition is constant, a small QD has a peak wavelength in the blue region that shifts gradually to the red region as the size increases.) The average size of red, green, and blue QD is around 5.8, 3.2, and 1.4 nm with 0.3 to 0.7 nm ZnS shell thickness, respectively, and the CdSe core region shows a zinc blende (sphalerite) structure. The peak positions of wavelength for red, green, and blue QD are 630, 540, and 450 nm, respectively. The CdSe/ZnS QDs were then spin-coated onto the poly-TPD and PEDOT:PSS-coated ITO glass. The red and green QDs were spin-coated at a rate of 1,800 rpm for 30 sec and the blue QD at 1,250 rpm for 30 sec (Fig. 1(c)). After baking at 80

Optics EXPRESS

°C for 30 minutes in the N_2-filled glove box, 2.5 wt% ZnO NPs (Nano Clean Tech) dispersed in mixed alcohol was spin-coated under ambient conditions at 2,000 rpm for 40 sec and baked at 110 °C for 10 min (Fig. 1(d)). A 100 nm-thick Al layer was deposited via thermal evaporation as the electrode on the ZnO layer (Fig. 1(e)). After fabrication of a standard QDLED, a 20-nm-thick MgF_2 layer was deposited on the Al electrode through e-beam evaporation to prevent sputtering damage to the Al electrode and ZnO layer (Fig. 1(f)). Then, a 5-nm-thick Ta layer was deposited to improve adhesion between the MgF_2 and the Co layer. Ten pairs of Co/Pt (1 nm/1.5 nm) and 10-nm-thick Ta layers were sequentially deposited on the adhesive Ta layer using DC sputtering, as shown in Fig. 2. The 10 nm-thick Ta layer was deposited on the FCPM to protect the FCPM from air oxidation. Both the Al electrode and the circular FCPM disks were fabricated with shadow masks during evaporation. The diameter of the circular disks and space between the disks

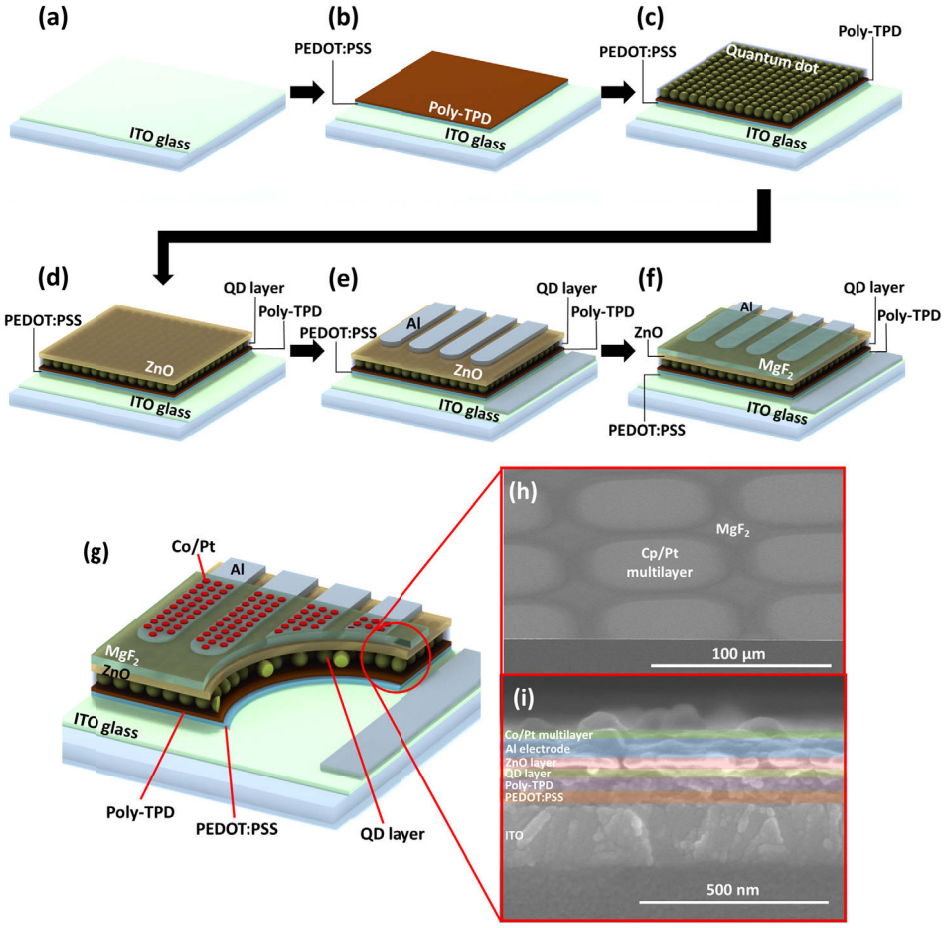

Fig. 1. Schematic of fabrication steps for QDLEDs with a ferromagnetic Co/Pt multilayer: (a) ITO-deposited glass substrate; (b) spin-coated PEDOT:PSS and poly-TPD as a hole transport layer on ITO glass; (c) spin coating of red, green, and blue quantum dots on hole transport layer in (b); (d) spin-coated ZnO as an electron transport layer on a QD layer; (e) thermally evaporated 100-nm-thick Al layer as an electrode on ZnO; (f) electron-beam-evaporated MgF_2 as an insulating and capping layer on Al and DC-sputtered ferromagnetic Co/Pt multilayer; (h) tilted and (i) cross-sectional scanning electron microscope (SEM) images of QDLED shown in (g).

Optics EXPRESS

were each 60 μm. Figure 1(f) shows the QDLED structure without circular FCPM disks; the structural sequence is ITO/PEDOT:PSS (~40 nm)/poly-TPD (~50 nm)/CdSe/ZnS core-shell QDs (~20 nm)/ZnO (~30 nm)/Al electrode (~100 nm)/MgF_2 (~20 nm). The full QDLED structure with circular FCPM disks is shown in Figs. 1(g) to 1(i). Figure 1(h) and 1(i) show a tilted angle and the cross-sectional scanning electron microscope (SEM) images of a QDLED with ferromagnetic Co/Pt multilayers. As shown in Fig. 1(i), the interface of the QDLED fabricated with a spin coating is not clearly distinguished. Therefore, we added colors to the SEM image to help identify each layer easily.

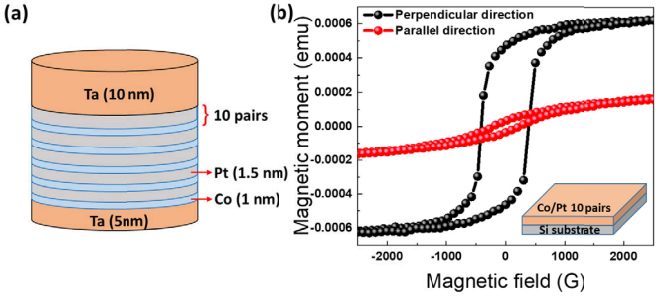

Fig. 2. (a) Schematic of the circular ferromagnetic Co/Pt multilayer disk structure, and (b) vibrating sample magnetometer (VSM) characteristics of ferromagnetic Co/Pt multilayer on a Si substrate. The inset shows a ferromagnetic Co/Pt multilayer film on a Si substrate (1×1 cm^2) for VSM measurements.

The structure of the Co/Pt multilayer is illustrated in Fig. 2(a). The Co and Pt layers were deposited via sputtering under optimized conditions for applying the perpendicular magnetic field to the QD layer. Typical ferromagnetic metals or alloys such as Fe, Ni, Nd, and CoFe require a magnetization process to align the magnetic field. Because this process requires a high temperature and vacuum with a strong external magnetic field, it is difficult to use in organic-based devices. Therefore, we used the FCPM because the alternately deposited Co and Pt layers spontaneously generate a magnetic field in a perpendicular direction without a magnetization process [23,24]. The thickness of the Co and Pt layers and number of Co/Pt pairs (Fig. 2(a)) were optimized by measuring the vibrating sample magnetometer (VSM), as shown in Fig. 2(b). When the Co thickness was too thin during sputtering, intermixing occurred between the Co and Pt layers. When it was too thick, the direction of the magnetic field gradually began to slant in the parallel direction from the perpendicular [25]. Therefore, the optimal FCPM magnetic moment was obtained using a 1 nm-thick Co layer and 1.5 nm-thick Pt layer within the 10 pairs of Co/Pt layers (Fig. 2(a)). The deposition rates of the Co and Pt layers were 0.171 and 0.176 Å/s, respectively. To confirm the magnetic field direction and strength of the FCPM, we measured the magnetic properties of an FCPM deposited on a 1×1 cm^2 Si substrate, as shown in the inset of Fig. 2(b). These magnetic field measurements were done using a VSM (Lake Shore Cryotronics). As a result, we obtained a remanent magnetic field of 0.18 T in the perpendicular direction and a negligibly small magnetic field in the parallel direction, as shown in Fig. 2(b).

The electrical and optical properties of the QDLED were obtained using a PR-650 spectrascan colorimeter (Photo Research) coupled with a Keithley 2400 source measurement unit. Inside the colorimeter, a photodetector was fixed at a distance of 355 mm from the QDLED. The light from the 14.5 mm^2 emitting area of the QDLED was collected using a light-focusing magnification lens. All of the electrical and optical property measurements were performed in the N_2-filled dark glove box to prevent stray light and oxidation at room temperature. In the TR-PL measurement, a pulsed 375 nm laser diode was used to excite the blue QDLED, and 473 nm was used for

Optics EXPRESS

the green and the red QDLEDs. A single-photon-counting photomultiplier tube was used for detection through the bottom side of the ITO glass.

3. Results and discussion

Figure 3 shows that luminescence increased after deposition of the circular FCPM disks on MgF_2. As shown in Fig. 1(g), the circular FCPM disks covered the Al electrodes of the red, green, and blue QDLEDs. Figures 3(a) to 3(c) show the current density–voltage (J–V) and luminance–voltage (L–V) characteristics of the red, green, and blue QDLEDs before and after FCPM deposition. The turn-on voltage for the red, green, and blue QDLEDs was the same at 3.0 V with and without circular FCPM disks. However, the series resistance of the QDLEDs slightly increased with the circular FCPM disks. The increase in resistance is due mainly to the altered carrier motion in the QDLEDs along the parallel direction caused by the perpendicular magnetic field and its gradient generated from the circular FCPM disks. The increase in resistance due to the magnetic field is already reported in InGaN/GaN MQWs, an AlGaN/GaN heterostructure, and an OLED [16,18,19]. After deposition of the circular FCPM disks, the luminescence of the red QDLED increased from 7,231 cd·m^{-2} to 10,842 cd·m^{-2} at 7.5 V (Fig. 3(a)). The luminescence of the green QDLEDs increased from 7,651 cd·m^{-2} to 9,852 cd·m^{-2} at 7.5 V (Fig. 3(b)) and that of the blue QDLEDs from 3,419 cd·m^{-2} to 4,106 cd·m^{-2} at 7.0 V (Fig. 3(c)). To further understand the changes in electrical and optical properties, we compared the current efficiency of the red, green, and blue QDLEDs before and after FCPM deposition at the maximum current

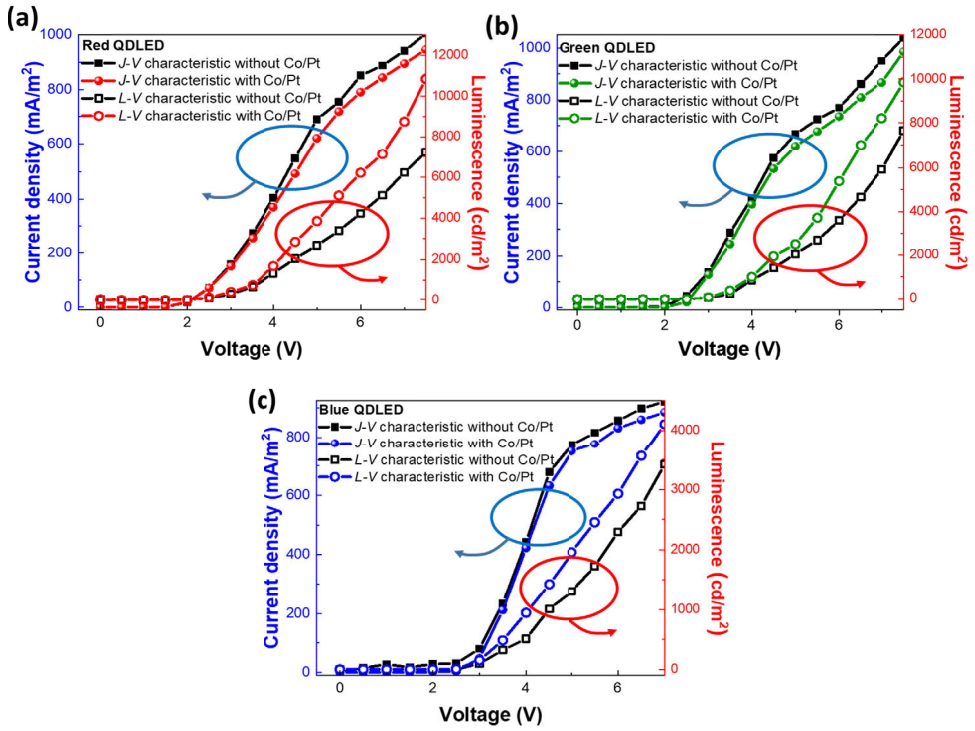

Fig. 3. (a) Current density–voltage (J–V) and luminance–voltage (L–V) characteristics of red, green, and blue QDLEDs before (black squares) and after (colored dots) deposition of the ferromagnetic Co/Pt multilayer (FCPM). J-V characteristics are plotted as solid squares (without FCPM) and solid dots (with FCPM). L-V characteristics are plotted as hollow squares (without of FCPM) and hollow dots (with FCPM).

Optics EXPRESS

injection and luminescence. The current efficiency of the red QDLED changed from 0.72 cd·A^{-1} to 1.15 cd·A^{-1} at 7.5 V, that of the green QDLED increased from 0.74 cd·A^{-1} to 1.0 cd·A^{-1} at 7.5 V, and that of the blue QDLED increased from 0.37 cd·A^{-1} to 0.6 cd·A^{-1} at 7.0 V. The enhancement of current efficiency is attributed to the simultaneous increase of luminescence and the change in electrical properties. This indicates that the magnetic fields enhance carrier injection into the QDs and carrier recombination in the QD layers.

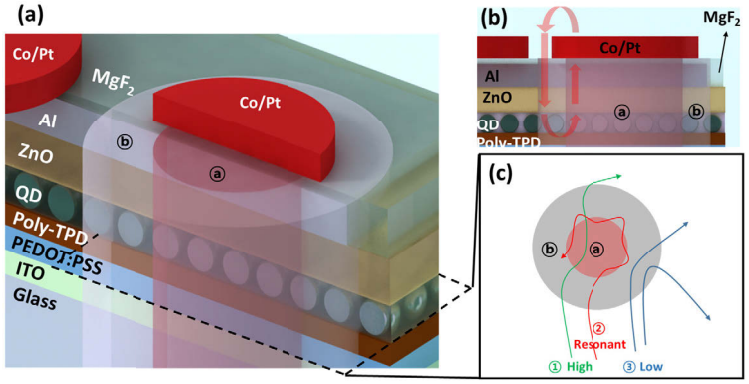

Fig. 4. Schematics of (a) tilted-angle and (b) front-angle cross-sectional view of a QDLED with a ferromagnetic Co/Pt multilayer and magnetic field profiles; (c) carrier motions under the perpendicular magnetic field and magnetic field gradients in the edge region (marked "a") where the magnetic field was strong and directed upward, and in the center region (marked "b") where the magnetic field was weak and directed downward. The carrier trajectories denoted by "1", "2", and "3" have high, resonant, and low kinetic energy under the magnetic field gradient, respectively.

As shown in Figs. 4(a) and 4(b), the perpendicular magnetic fields generated by the circular disks of ferromagnetic Co/Pt multilayers are strong at the edge region where the field direction downward and relatively weak at the center region where the field direction upward [14,15]. Consequently, the magnetic field gradient is created, as shown in Fig. 4(b). The kinetic energy of a carrier and the position at which the carrier enters the magnetic field determine its trajectory based on the magnetic field gradient. When the carriers enter a region of the strong or weak magnetic field, denoted respectively by "b" and "a" in Figs. 4(a) to 4(c), they will be scattered or trapped depending on the carrier kinetic energy. Carriers with high kinetic energy can penetrate the edge (outer core) and the center (inner core) regions and reach the opposite side of the outer core again. In this case, the carrier exhibits a helical motion while passing through the magnetic field region, and is scattered in a random direction (1 in Fig. 4(c)). However, Carriers with low kinetic energy cannot enter through the edge region of the circular disk where the magnetic field is strong, and they will be scattered backward (3 in Fig. 4(c)). When carriers with the appropriate kinetic energy (i.e., resonant energy) pass through the outer core region, they move along the interface between the inner and outer cores with a snaking motion (2 in Fig. 4(c)) [14]. The increase of the series resistance of QDLEDs with FCPM in Figs. 3(a)–3(c) is owing to carrier scattering or temporal trapping [14,26,27].

In organic-based LEDs, the mobility of holes is faster than electrons and the effective mass of holes is about 10-20% heavier than electrons. [28]. In general, carrier trajectories such as the radius of the helical motion, the direction of propagation, and the direction of rotation are mainly effected by effective mass, magnetic field strength, and gradient of the magnetic field. Also, the carrier velocity under the magnetic field is determined by the carrier effective mass, magnetic field strength, and magnetic field gradient [29]. Therefore, the electron and the hole

Optics EXPRESS

under the same strength and gradient of the magnetic field exhibit little difference in radius of helical motion due to the similar effective mass, but the direction of rotation and propagation are contrary to each other because of their opposite charges. Accordingly, the carrier density around each QD increased due to lateral diffusion of the carrier, and the probability of radiative recombination increased because of the perpendicular magnetic field localized carriers in the QD. Furthermore, the magnetic field strongly localizes carriers in QDs, which increases radiative recombination. The stronger carrier localization minimizes ejection of carriers from the QD core region through thermal release [9,12]. In fact, carriers receive sufficient thermal energy to escape from a QD even below room temperature [10]. The released carriers enter the nonradiative recombination center and reduce the QD efficiency. This is why the enhanced EL intensity of the QDLEDs is due to the increased carrier localization in QDs by the perpendicular magnetic field and its gradient.

The luminescence of the red, green, and blue QDLEDs increased by 33.31%, 22.34%, and 16.73%, respectively, after deposition of the circular FCPM disks, as shown in Fig. 3. The red QD is larger than the green and blue QDs, so an increase of luminescence enhances with QD size. This shows that the magnetic field gradient affects larger QDs more. This is because QD size determines the carrier capturing potential [8]. Although the magnetic field intensity produced by the circular FCPM disks is the same for all QDs, the magnetic field gradient localizes more carriers in larger QDs because such QDs have sufficient room to trap more carriers in their cores.

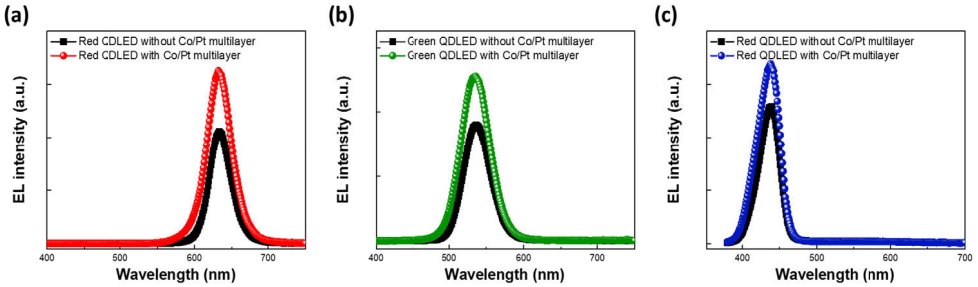

Fig. 5. EL spectra of (a) red, (b) green, and (c) blue QDLEDs without (black squares) and with (colored dots) deposition of the ferromagnetic Co/Pt multilayer.

Figure 5 shows the FWHM of the QDLED EL before and after deposition of the circular FCPM disks. After deposition, the FWHM of the red QDLED increased by 4.22 nm (from 33.77 nm to 37.99 nm) at 7.5 V and that of the green by 3.84 nm (from 41.45 nm to 45.29 nm) at 7.5 V. The FWHM of the blue QDLED increased by 4.15 nm (from 32.43 nm to 36.58 nm) at 7.0 V. The FWHM of the EL spectra for all QDLEDs after disk deposition increases in proportion to QD size. It has been reported that the FWHM of a QD broadens under an external magnetic field [8,30]. This broadening is attributed to energy level splitting by the Zeeman effect or localization of the surface defect and core–shell interface by the magnetic field [10,30,31]. The QD energy level is split and the degeneracies removed when a magnetic field is applied to the QDs. In addition, strong localization by the magnetic field causes carrier trapping at a shallow potential, as shown by the fluctuation in QD surface composition and defects at the core–shell interface. As a result, the emission spectra of the QDLEDs with circular FCPM disks become broader than those without these disks, as shown in Fig. 5. When the magnetic field is applied to the QD, the spatial confinement increases as the QD size decreases, thereby increasing the interlevel separation. Therefore, even if the magnetic field strength is constant, the energy level separation by the Zeeman effect increases as the QD size decreases. As a result, the EL spectrum becomes broader as the QD size decreases [8,32]. However, although the FWHM increased after FCPM deposition, it did not change with size in this study. Because energy level splitting strongly

Optics EXPRESS

depends on magnetic field strength, a stronger magnetic field is needed to verify the changes in FWHM due to QD size.

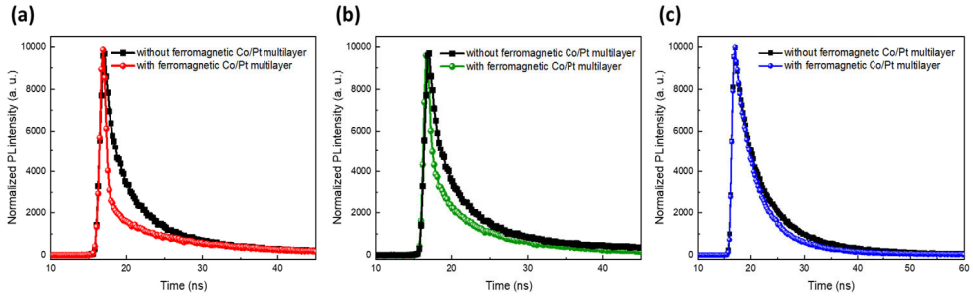

Fig. 6. TR-PL spectra without (black squares) and with (colored dots) a ferromagnetic Co/Pt multilayer for the (a) red, (b) green, and (c) blue QDLEDs.

We performed TR-PL measurement to further understand the effect of the magnetic field gradient on the optical properties of the QDLEDs. Figure 6 shows the TR-PL decay times before and after FCPM disk deposition. The TR-PL decay time of the red QD decreased from 3.24 ns to 2.23 ns, that of the green QD from 4.00 ns to 3.19 ns, and that of the blue QD from 3.57 ns to 3.14 ns. The reduced decay times reveal that the carriers were strongly localized in the QDs and recombined more efficiently [33]. Therefore, the enhanced QDLED luminescence is due primarily to the strong localization of carriers in the QD caused by the circular FCPM disks. Furthermore, the decrease in decay time was greatest in the red QDLED and smallest in the blue QDLED. This is another indication that the effect of the magnetic field gradient generated from the FCPM disks is greater in QDLEDs with larger QDs because the carriers are strongly localized and recombine more efficiently in them.

4. Conclusion

In summary, we have enhanced the luminescence of red, green, and blue QDLEDs by depositing circular FCPM disks on top of the MgF_2 capping layer of an Al electrode. The circular FCPM disks increased the EL intensities of the red, green, and blue QDLEDs by 33.31%, 22.34%, and 16.73%, respectively, compared with QDLEDs without the disks. The EL intensity increased because the magnetic field and its gradient produced by the FCPM disks changed the trajectory of carriers, thereby enhancing carrier injection into QDs. In addition, the magnetic field gradient suppressed carrier loss from thermal release through localization. On the basis of FWHM and TR-PL measurements of the EL spectra, we conclude that the increase in QDLED EL is due mostly to the magnetic field and its gradient. Furthermore, a shorter TR-PL decay time reveals more efficient carrier recombination due to the suppressed carrier escape through increased localization. Improving QDLED luminescence using a perpendicular magnetic field from circular FCPM disks may be an alternative way to design high-efficiency QDLEDs.

Funding

National Research Foundation of Korea (NRF-2017R1A2B2011858); "Amano Center for Advanced LEDs" of Gwangju Institute of Science and Technology.

Disclosures

The authors declare no conflicts of interest.

Optics EXPRESS

References

1. Y. Shirasaki, G. J. Supran, M. G. Bawendi, and V. Bulović, "Emergence of colloidal quantum-dot light-emitting technologies," Nat. Photonics **7**(1), 13–23 (2013).
2. B. S. Mashford, M. Stevenson, Z. Popovic, C. Hamilton, Z. Zhou, C. Breen, J. Steckel, V. Bulovic, M. Bawendi, S. Coe-Sullivan, and P. T. Kazlas, "High-efficiency quantum-dot light-emitting devices with enhanced charge injection," Nat. Photonics **7**(5), 407–412 (2013).
3. S. Kim, S. H. Im, and S. W. Kim, "Performance of light-emitting-diode based on quantum dots," Nanoscale **5**(12), 5205–5214 (2013).
4. Q. Sun, Y. A. Wang, L. S. Li, D. Wang, T. Zhu, J. Xu, C. Yang, and Y. Li, "Bright, multicoloured light-emitting diodes based on quantum dots," Nat. Photonics **1**(12), 717–722 (2007).
5. J. Kwak, W. K. Bae, D. Lee, I. Park, J. Lim, M. Park, H. Cho, H. Woo, D. Y. Yoon, K. Char, S. Lee, and C. Lee, "Bright and efficient full-color colloidal quantum dot light-emitting diodes using an inverted device structure," Nano Lett. **12**(5), 2362–2366 (2012).
6. W. K. Bae and J. Lim, "Nanostructured colloidal quantum dots for efficient electroluminescence devices," Korean J. Chem. Eng. **36**(2), 173–185 (2019).
7. Q. Zhang, X. Gu, Z. Chen, J. Jiang, Z. Zhang, J. Wei, F. Li, X. Jin, Y. Song, and Q. Li, "Enhancing extraction efficiency of quantum dot light-emitting diodes by surface engineering," Opt. Express **25**(15), 17683–17694 (2017).
8. M. S. Kushwaha, "Magneto-optical absorption in semiconducting spherical quantum dots: Influence of the dot-size, confining potential, and magnetic field," AIP Adv. **4**(12), 127151 (2014).
9. G. Weng, W. R. Zhao, S. Q. Chen, H. Akiyama, Z. C. Li, J. P. Liu, and B. P. Zhang, "Strong localization effect and carrier relaxation dynamics in self-assembled InGaN quantum dots emitting in the green," Nanoscale Res. Lett. **10**(1), 31 (2015).
10. P. Jing, J. Zheng, M. Ikezawa, X. Liu, S. Lv, X. Kong, J. Zhao, and Y. Masumoto, "Temperature-dependent photoluminescence of CdSe-core CdS/CdZnS/ZnS-multishell quantum dots," J. Phys. Chem. C **113**(31), 13545–13550 (2009).
11. B. N. Pal, Y. Ghosh, S. Brovelli, R. Laocharoensuk, V. I. Klimov, J. A. Hollingsworth, and H. Htoon, "Giant CdSe/CdS core/shell nanocrystal quantum dots as efficient electroluminescent materials: strong influence of shell thickness on light-emitting diode performance," Nano Lett. **12**(1), 331–336 (2012).
12. M. Larsson, E. Moskalenko, A. Larsson, P. Holtz, C. Verdozzi, C.-O. Almbladh, W. V. Schoenfeld, and P. M. Petroff, "Magnetic field effects on optical and transport properties in InAs/GaAs quantum dots," Phys. Rev. B **74**(24), 245312 (2006).
13. E. Alphandéry, R. J. Nicholas, N. J. Mason, S. G. Lyapin, and P. C. Klipstein, "Photoluminescence of self-assembled InSb quantum dots grown on GaSb as a function of excitation power, temperature, and magnetic field," Phys. Rev. B **65**(11), 115322 (2002).
14. J. Reijniers, F. M. Peeters, and A. Matulis, "Electron scattering on circular symmetric magnetic profiles in a two-dimensional electron gas," Phys. Rev. B **64**(24), 245314 (2001).
15. A. Nogaret, S. J. Bending, and M. Henini, "Resistance resonance effects through magnetic edge states," Phys. Rev. Lett. **84**(10), 2231–2234 (2000).
16. Q. X. Zhao, B. Monemar, P. O. Holtz, T. Lundström, M. Sundaram, J. L. Merz, and A. C. Gossard, "Magnetic-field-induced localization effects on radiative recombination in GaAs/$Al_xGa_{1-x}As$ heterostructures," Phys. Rev. B **50**(11), 7514–7517 (1994).
17. F. Y. Tsai, C. P. Lee, O. Voskoboynikov, H. H. Cheng, J. Shen, and Y. Oka, "Time-resolved photoluminescence study of InGaAs/GaAs quantum wells on (111)B GaAs substrates under magnetic fields," J. Appl. Phys. **89**(12), 7875–7878 (2001).
18. B. Arnaudov, T. Paskova, O. Valassiades, P. P. Paskov, S. Evtimova, B. Monomer, and M. Heuken, "Magnetic-field-induced localization of electrons in InGaN/GaN multiple quantum wells," Appl. Phys. Lett. **83**(13), 2590–2592 (2003).
19. J. J. Kim, Y. C. Leem, J. W. Kang, J. Kwon, B. Cho, S. Y. Yim, J. H. Baek, and S. J. Park, "Enhancement of the Optical Output Power of InGaN/GaN Multiple Quantum Well Light-Emitting Diodes by a CoFe Ferromagnetic Layer," ACS Photonics **2**(11), 1519–1523 (2015).
20. B. Hu, L. Yan, and M. Shao, "Magnetic-field effects in organic semiconducting materials and devices," Adv. Mater. **21**(14-15), 1500–1516 (2009).
21. J. Kalinowski, M. Cocchi, D. Virgili, P. D. Marco, and V. Fattori, "Magnetic field effects on emission and current in Alq_3-based electroluminescent diodes," Chem. Phys. Lett. **380**(5-6), 710–715 (2003).
22. C. J. Sun, Y. Wu, Z. Xu, B. Hu, J. Bai, J. P. Wang, and J. Shen, "Enhancement of quantum efficiency of organic light emitting devices by doping magnetic nanoparticles," Appl. Phys. Lett. **90**(23), 232110 (2007).
23. N. Nakajima, T. Koide, T. Shidara, H. Miyauchi, H. Fukutani, A. Fujimori, K. Iio, T. Katayama, M. Nývlt, and Y. Suzuki, "Perpendicular Magnetic Anisotropy Caused by Interfacial Hybridization via Enhanced Orbital Moment in Co/Pt Multilayers: Magnetic Circular X-Ray Dichroism Study," Phys. Rev. Lett. **81**(23), 5229–5232 (1998).
24. S. Bandiera, R. C. Sousa, B. Rodmacq, and B. Dieny, "Asymmetric interfacial perpendicular magnetic anisotropy in Pt/Co/Pt trilayers," IEEE Magn. Lett. **2**, 3000504 (2011).
25. J. Thiele, C. Boeglin, K. Hricovini, and F. Chevrier, "Magnetic circular x-ray-dichroism study of Co/Pt (111)," Phys. Rev. B **53**(18), R11934 (1996).

Optics EXPRESS

26. J. H. Han, J. J. Kim, Y. C. Leem, S. J. Kim, W. Kwak, W. L. Jeong, B. Cho, D. S. Lee, and S. J. Park, "Improved efficiency of InGaN/GaN light-emitting diodes with perpendicular magnetic field gradients," *Opt. Express* (accepted).
27. K. S. Novoselov, A. K. Geim, S. V. Dubonos, Y. G. Cornelissens, F. M. Peeters, and J. C. Maan, "Scattering of ballistic electrons at a mesoscopic spot of strong magnetic field," Phys. Rev. B **65**(23), 233312 (2002).
28. O. Ostroverkhova, *Handbook of Organic Materials for Electronic and Photonic Devices* (Elsevier, 2019).
29. F. F. Chen, *Introduction to plasma physics and controlled fusion* (Plenum Press, 1984).
30. S. Raymond, S. Fafard, P. J. Poole, A. Wojs, P. Hawrylak, C. Gould, A. Sachrajda, and S. Charbonneau, "State-filling and magneto-photoluminescence of excited states in InGaAs/GaAs self-assembled quantum dots," Superlattices Microstruct. **21**(4), 541–558 (1997).
31. Q. Ren, L. Bai, A. Murayama, Z. Chen, and X. Shen, "Magnetic field induced charging effect in a single CdSe quantum dot," Phys. Status Solidi B **246**(4), 791–794 (2009).
32. S. J. Prado, C. Trallero-Giner, A. M. Alcalde, V. López-Richard, and G. E. Marques, "Influence of quantum dot shape on the Landé g-factor determination," Phys. Rev. B **69**(20), 201310 (2004).
33. Y. Gao and X. Peng, "Photogenerated excitons in plain core CdSe nanocrystals with unity radiative decay in single channel: the effects of surface and ligands," J. Am. Chem. Soc. **137**(12), 4230–4235 (2015).